Chapter 2
Anatomy of the Carotid Artery

J. Scott McNally and Michael McLaughlin

Anatomy of the Carotid Artery

The Carotid Space

The left and right carotid spaces are paired tubular spaces contained in a fascial sheath made up of the three deep cervical fascia layers. The carotid space contains the carotid arteries, carotid body, carotid sinus, internal jugular (IJ) veins as well as cranial nerves (CN) IX-XII. The internal jugular nodal chain is associated with the outer sheath, but there are no nodes located within the carotid space itself.

In the suprahyoid neck, the sheath is more incomplete than in the infrahyoid neck. Multiple cranial nerves are present within the suprahyoid carotid sheath including CN IX-XII. Only CN X remains in the infrahyoid neck where the nerve is located in the posterior notch between the ICA and IJ. The sympathetic plexus is found along the posterior aspect of the carotid sheath closely opposed to the prevertebral fascia. The ansa cervicalis is part of the cervical plexus of nerves forming a loop located within the anterior wall of the carotid sheath. The superior root descending over the ICA/CCA is a continuation of CN XII with fibers from the C1 spinal nerve supplying the superior belly of the omohyoid. The inferior root descends around the IJ with C2-C3 spinal nerve fibers and supplies the inferior belly of the omohyoid. The inferior root joins the superior root anteriorly and inferiorly along the CCA to form the ansa cervicalis, which supplies the sternohyoid and sternothyroid muscles.

There are two additional important structures within the carotid sheath, the carotid body and carotid sinus. The carotid body is a chemoreceptor consisting of two types of receptor cells: (1) **Type I cells** (glomus cells) that are derived from the

J. S. McNally (✉) · M. McLaughlin
Department of Radiology, University of Utah Health System, Salt Lake City, UT, USA
e-mail: scott.mcnally@hsc.utah.edu; Michael.McLaughlin@hsc.utah.edu

M. S. Park et al. (eds.), *Carotid Artery Disease*,
https://doi.org/10.1007/978-3-030-41138-1_2

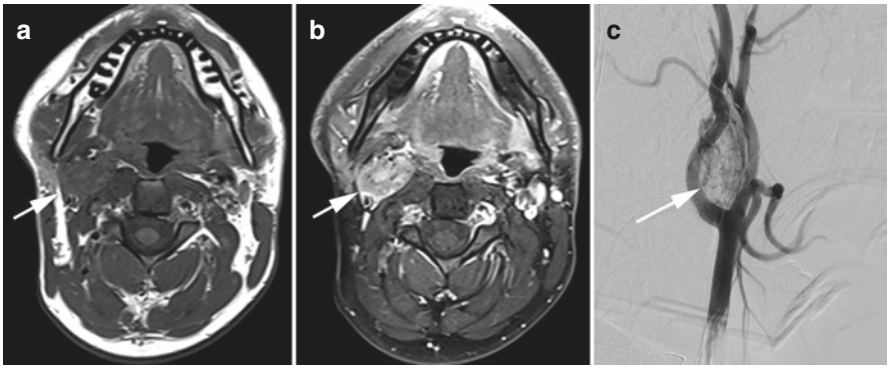

Fig. 2.1 Carotid body paraganglioma. Right carotid body paraganglioma on MRI, with T1 precontrast (**a**), T1 postcontrast (**b**), and pretreatment DSA (**c**) showing an avidly enhancing mass (arrow) splaying the internal and external carotid artery

neural crest and release acetylcholine, ATP, and dopamine when activated, and (2) **Type II cells** (sustentacular cells) which serve as supporting cells. The carotid body monitors blood pH, pCO_2, and pO_2 and senses acidemia, hypercapnia, or hypoxia, respectively. The carotid body can increase sympathetic tone to increase blood pressure, heart rate, and respiratory rate. The carotid body is normally ≤6 mm in size on imaging, but when larger raises the concern for a carotid body paraganglioma (Fig. 2.1) [1]. It is innervated by the carotid sinus nerve, a branch of CN IX that provides sensory innervation. Nerve fibers travel to the nucleus tractus solitarii (NTS) in the medulla oblongata and indirectly modulate sympathetic and parasympathetic tone in the medulla and pons via the hypothalamus. The cell bodies of the afferent neurons reside in the petrosal ganglion and synapse with type I cells. Because this region contains an important baroreceptor and chemoreceptor, avoiding carotid sinus nerve and carotid body during endarterectomy is important to preserve autonomic function [2]. The carotid body is also the target for carotid massage, which can decrease both heart rate and blood pressure. While carotid stimulation can induce bradycardia and even syncope in some individuals, fatal cardiac events following carotid sinus stimulation are rare and often accompanied by the presence of drug abuse and/or cardiac pathology, and may be secondary to underlying predispositions as opposed to the stimulation itself [3].

Carotid Artery Anatomy and Predisposition to Atherosclerosis

Carotid artery anatomy is essential to the understanding of plaque predilection to the carotid bifurcation. Like all arteries, the carotid consists of 3 layers (from inner to outer): tunica intima, media, and adventitia. The intima consists of a single layer of endothelial cells with a collagen matrix underneath. The media consists of a thick layer of vascular smooth muscle cells (VSMC) and matrix. The adventitia is

composed of fibroblasts and adipocytes. Vasa vasorum are found in the carotid artery, primarily located near the bifurcation and bulb, and these course within the adventitia penetrating into the media and nearly reaching the intima [4]. Patients with atherosclerosis have a higher density of vasa vasorum, and the endothelial lining of these small vessels may represent a potential atherosclerosis prevention or treatment target [5].

As a result of their prime location, endothelial cells experience three types of mechanical force: pressure, circumferential stretch, and shear stress or the dragging force created by blood flow. Of these, shear stress may be the most important due to the modulation of genes and controlled release of vasoactive substances [6]. For over a century, pathologists have known atherosclerosis does not occur randomly throughout the vasculature. Instead, plaque occurs at specific anatomic locations such as branch points and non-linear vascular segments. In particular, the outer wall of the carotid artery is highly predisposed to atherosclerotic plaque, and is located 180 degrees opposite the flow divider at the bifurcation and bulb. Blood flow at the carotid bifurcation is non-laminar, in contrast to linear vascular segments.

Linear vessel segments experience laminar flow and are relatively protected from atherosclerosis [7]. Laminar shear stress stimulates endothelial nitric oxide (NO) production, and this accounts for the main atheroprotective effect of aerobic exercise [8]. During exercise, NO causes vasodilation and increased perfusion of downstream tissues. Importantly, NO also counteracts atherogenesis by inhibiting platelet aggregation, VSMC proliferation, leukocyte adhesion, and oxidative damage [9]. Through this mechanism, exercise counteracts the proatherosclerotic conditions of hypertension, diabetes, and hypercholesterolemia which can disrupt endothelial response to laminar shear stress [10, 11].

In contrast, at the carotid bifurcation flow reversal and oscillatory shear stress occur during systole along the outer wall of the carotid bulb. This site is particularly prone to intima-media thickening and atherosclerosis [12, 13]. Studies have shown that early carotid plaque formation is related to an oscillating pure positive and negative shear stress, as opposed to disorganized turbulent flow. In cell culture models, this oscillatory shear stress increases superoxide and oxidase activity [14–16] and correspondingly decreases NO levels [17]. Decreased NO contributes to atherogenesis by increased inflammation, vasoconstriction, VSMC proliferation, leukocyte adhesion, coagulation, and increased oxidative damage. This accounts for the predilection of plaque along the outer wall of the carotid bulb.

Extracranial Arterial Anatomy

Arch Anatomy

There are both left and right common carotid arteries (CCA) with a similar course in the neck, but with different origins. The normal aortic arch configuration of the great vessel origins includes (from right to left) the brachiocephalic, left CCA

and left subclavian arteries. The brachiocephalic artery bifurcates into the right subclavian artery and right CCA. Variations on this anatomy occur, most often related to a common origin of the brachiocephalic and left CCA (often referred to as a“bovine-type” arch, though this bears no resemblance to the bovine arch), direct arch origin of the left vertebral artery, or aberrant right subclavian artery (ARSA) with a retroesophageal course [18]. Congenital aortic arch variants may have important clinical implications as they can be associated with vascular rings, congenital heart disease, and chromosomal abnormalities.

CCA Anatomy

Both CCA's are symmetric in their course and are contained within the carotid sheath. This sheath is in contiguity with the deep cervical fascia and serves as the boundary of the carotid space. In males the average CCA diameter is 6.5 mm and in females is 6.1 mm [19].

Carotid Triangle

The carotid triangle is formed when the sternocleidomastoid is retracted posteriorly. The posterior margin of the triangle is formed by the sternocleidomastoid, the stylohyoid and posterior belly of the digastric muscles the superior margin, and the superior belly of the omohyoid forms the inferior margin. In this triangle, CN XII crosses superficial to the carotid artery (sometimes within the carotid sheath) obliquely from posterosuperiorly to anteroinferiorly.

Carotid Bifurcation and Bulb

The carotid bifurcation occurs at approximately the C4 vertebral body level in most patients, though can be seen as low as T2 or as high as C1-C2. The CCA bifurcates into the internal carotid artery (ICA) and external carotid artery (ECA). In most patients, the ICA originates posterolaterally and the ECA originates anteromedially, though the reverse can be seen about 10% of the time. The bifurcation is mobile and can turn within the sheath during swallowing or vocalization, and the orientation of the ICA-ECA can change between imaging scans (Fig. 2.2). Superior to the bifurcation there is a normal anatomic dilation known as the carotid bulb. Very rarely, there is no bulb and the ECA branches arise directly from the CCA.

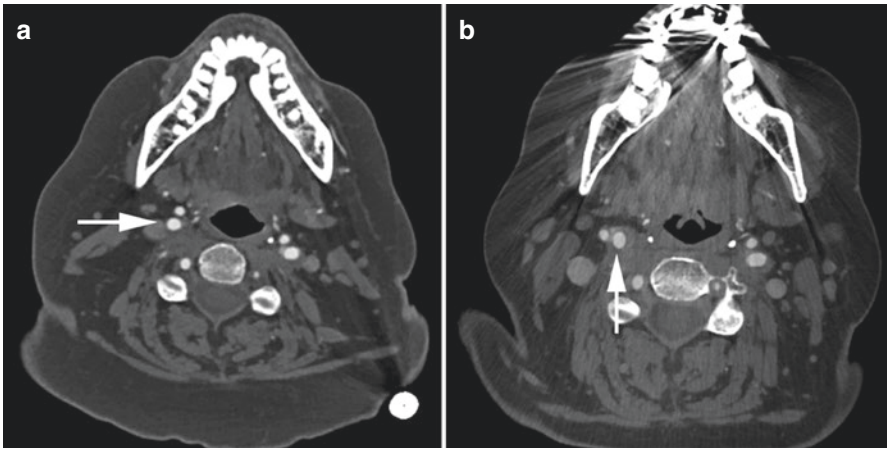

Fig. 2.2 Carotid bifurcation rotation. Two CTA scans 6 months apart showing rotation of the right carotid bifurcation within the carotid sheath. Initially, the right ICA (arrow) was located posterolateral to the ECA (**a**). On the second scan, the right carotid rotated such that the ICA (arrow) was located medial to the ECA (**b**)

External Carotid Artery (ECA)

The ECA is named for external course, and can be distinguished from the ICA by its multiple branches. Potential anastomotic routes can exist between the extracranial and intracranial arteries, so called 'dangerous' anastomoses due to the potential for non-target embolization to the central nervous system during ECA intervention procedures involving the skull base and orbit [20, 21]. The 8 named branches of the ECA are: **superior thyroid, ascending pharyngeal, lingual, facial, occipital, posterior auricular, superficial temporal, and internal maxillary arteries**. These branches supply facial structures and are named according to the structure they supply or their anatomic course:

Superior Thyroid Artery

Usually this is the first ECA branch, though sometimes it arises directly from the CCA below or near the bifurcation. This artery courses inferiorly to supply the superior thyroid gland and larynx, and anastomoses with the inferior thyroid artery arising from the thyrocervical trunk. A rare example of a superior thyroid infarct is shown in Fig. 2.3.

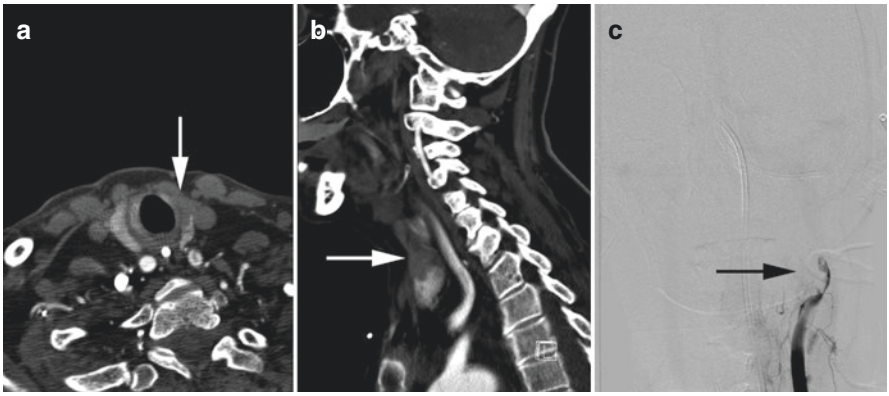

Fig. 2.3 Superior thyroid infarction. Patient with acute left hemispheric infarction related to left carotid occlusion involving both the ECA and ICA. Thrombus extended into the left superior thyroid artery resulting in superior thyroid lobe infarction (white arrows) on axial (**a**) and sagittal CTA (**b**). DSA with delayed imaging confirmed left ICA and ECA occlusion (**c**, black arrow)

Ascending Pharyngeal Artery

This artery is often the second ECA branch though can have a variant origin at the notch of the carotid bifurcation. This vessel courses superiorly between the ICA/ECA and supplies the nasopharynx and oropharynx. Muscular/tympanic branches supply the pharyngotympanic (Eustachian) tube, middle ear and prevertebral musculature. Neuromeningeal branches supply cranial nerves IX-XI and the dura. Potentially dangerous anastomoses are present with the middle/accessory meningeal caroticotympanic and Vidian arteries. An example of an enlarged ascending pharyngeal artery in the setting of an anatomic variant aberrant ICA is shown in Fig. 2.4. In this case, the ascending pharyngeal artery supplies an enlarged inferior tympanic artery, caroticotympanic artery, and then connects with the posterolateral aspect of horizontal petrous ICA.

Lingual Artery

Usually the second ECA branch, the lingual artery courses anteroinferiorly and is the major vascular supply to the tongue, oral cavity and submandibular gland. In some cases the lingual and facial arteries can arise from a common origin.

Facial Artery

The facial artery arises superior to the lingual artery and courses along the cheek to supply the face, lip and cheek as well as the palate. There are potentially dangerous anastomoses along the anterior cheek with the ophthalmic artery branch of the ICA.

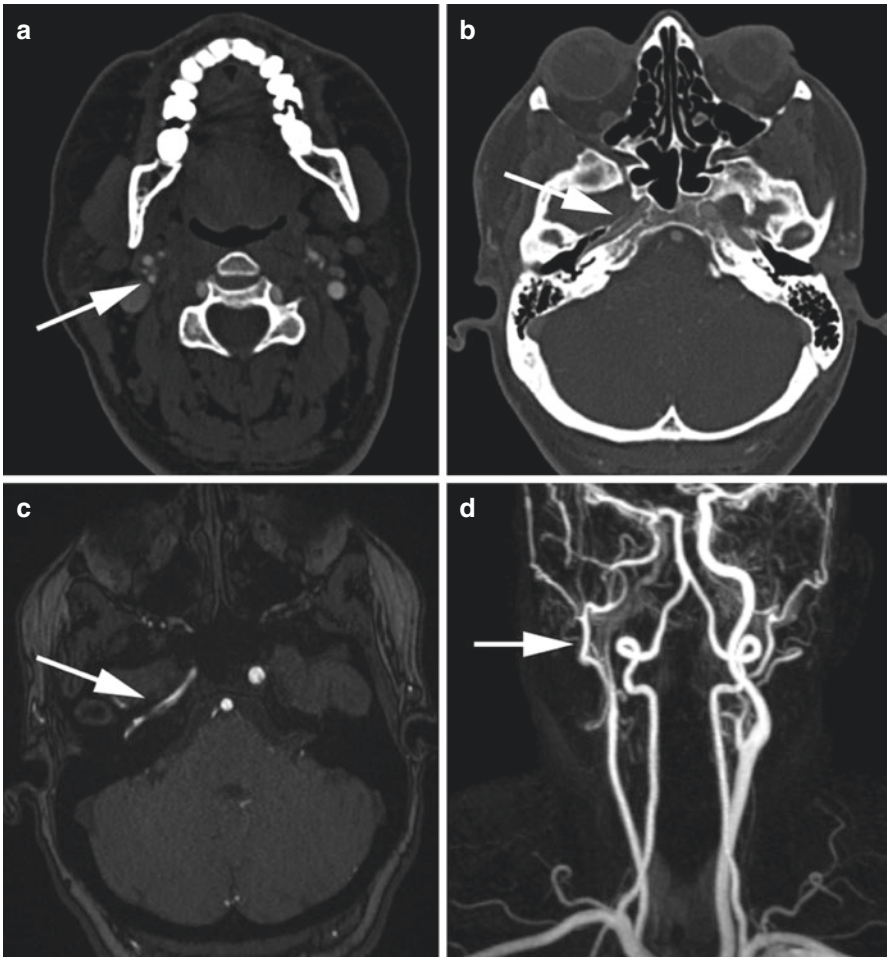

Fig. 2.4 Aberrant internal carotid artery. Patient with an aberrant right ICA. CTA showed an enlarged right-sided ascending pharyngeal artery (**a**, arrow) that coursed along the cochlear promontory with an asymmetrically small carotid canal (**b**, arrow). The ascending pharyngeal artery supplied an enlarged inferior tympanic artery, caroticotympanic artery, and then connected with the posterolateral aspect of horizontal petrous ICA. MRA with TOF (**c**) and contrast maximum intensity projections (**d**) confirmed an aberrant right ICA (arrow)

Occipital Artery

This artery arises from the posterior ECA and courses posteriorly to supply the occipital scalp, upper cervical musculature and dura of the posterior fossa with multiple potential dangerous anastomoses with the vertebral arteries through muscular branches. This artery serves as important embolic access for posterior fossa meningiomas and dural arteriovenous fistulae (dAVF) which commonly occur at the margin of the transverse/sigmoid sinus junction. An example of an

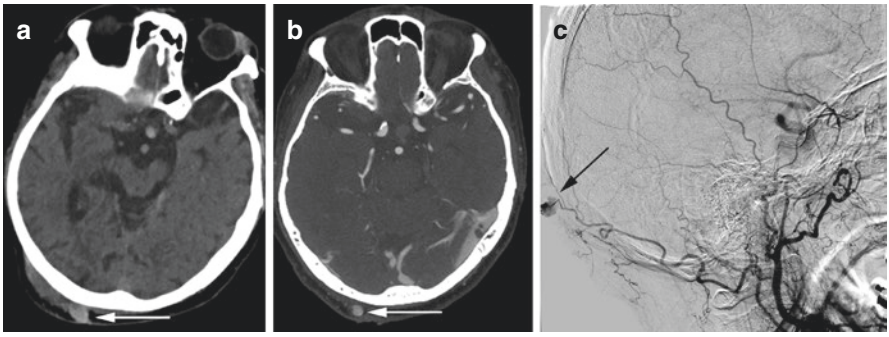

Fig. 2.5 Occipital artery pseudoaneurysm. Patient with a right occipital scalp laceration after ground level fall. Noncontrast CT showed a rounded hematoma along the right occipital scalp (**a**, arrow). The hematoma began to pulsate, and CTA was performed which showed a pseudoaneurysm (**b**, arrow). DSA confirmed the pseudoaneurysm was supplied by the occipital artery (**c**, arrow). This was subsequently embolized

occipital artery pseudoaneurysm related to prior trauma is shown in Fig. 2.5, subsequently treated with embolization.

Posterior Auricular Artery

This branch arises superior to the occipital artery origin and courses posteriorly to supply the pinna of the ear, posterior scalp, external auditory canal and chorda tympani.

Superficial Temporal Artery (STA)

The smaller of the terminal ECA branches is the superficial temporal artery, which courses posteroinferiorly to the mandibular condyle to supply the scalp. This vessel is often biopsied in cases of suspected ECA vasculitis and can present with pseudoaneurysms as shown in Fig. 2.6. An additional case of an STA fistula from stabbing is shown in Fig. 2.7.

(internal) Maxillary Artery (iMAX)

The largest terminal ECA branch is the iMAX, which arises deep to the mandibular condylar neck in the parotid space. The iMAX branches include the middle meningeal artery (MMA) and the sphenopalatine branch. The MMA is an important

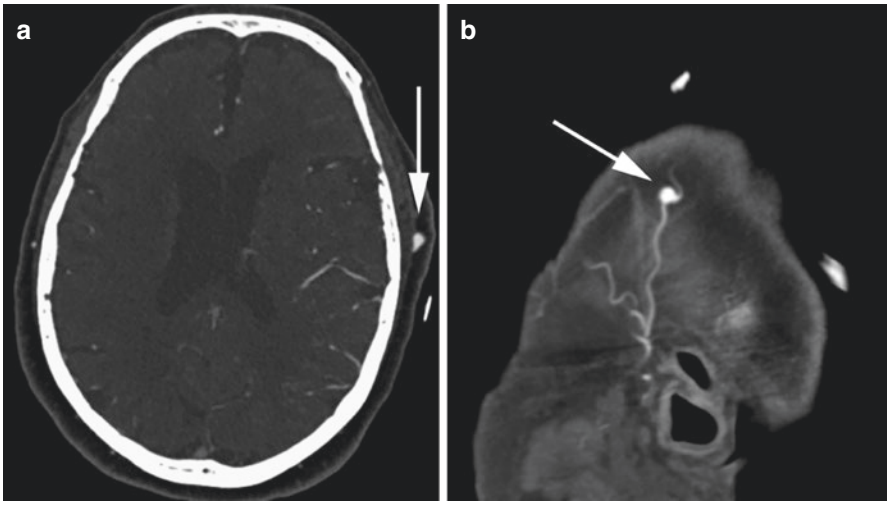

Fig. 2.6 Superficial temporal artery vasculitis and pseudoaneurysm. Patient with headache and vision loss who underwent workup with CTA. Axial (**a**) and sagittal CTA images (**b**) showed a 5 mm left sided superficial temporal artery pseudoaneurysm and the patient subsequently went to biopsy confirming giant cell arteritis

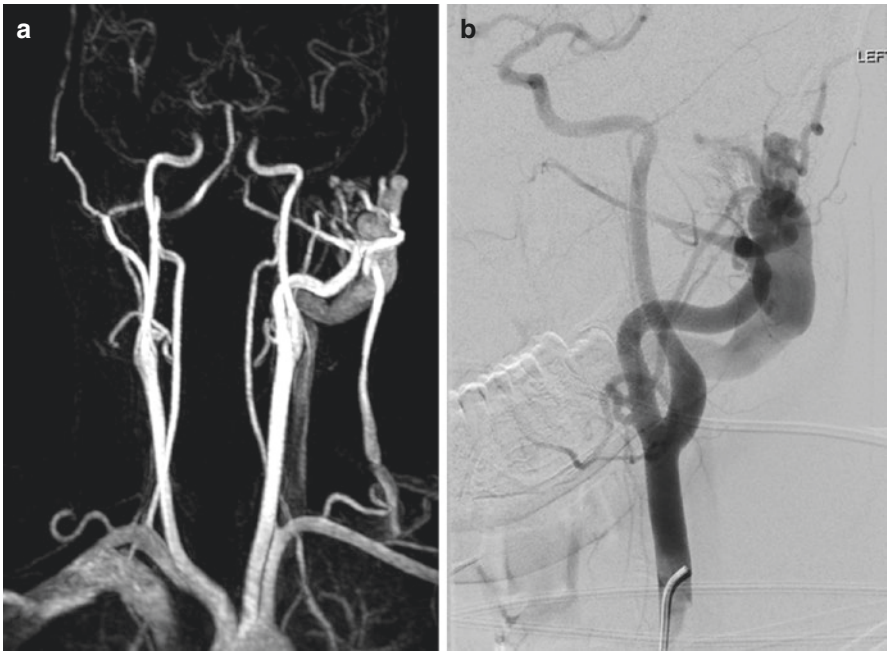

Fig. 2.7 Superficial temporal arteriovenous fistula. Patient with a pulsatile mass at the site of a prior stab wound. MRA (**a**) showed arteriovenous shunting within the left parotid mass, which was found to represent a posttraumatic arteriovenous fistula on DSA (**b**)

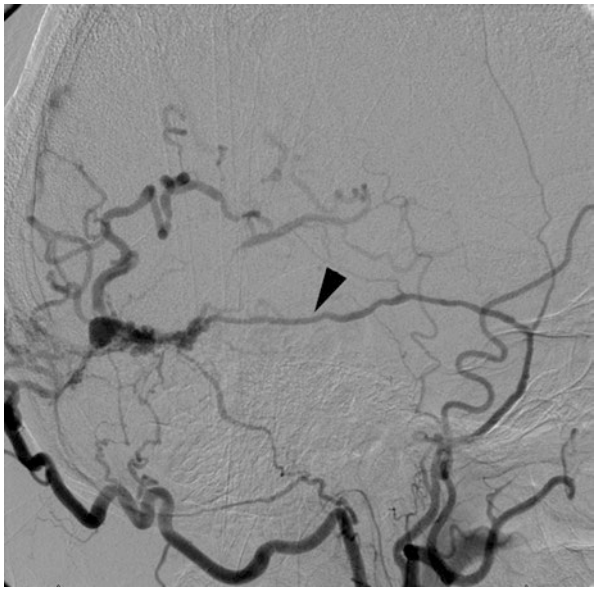

Fig. 2.8 Dural arteriovenous fistula. Patient who presented with worsening left sided headache and vision loss. DSA shows a left sided dural arteriovenous fistula fed by multiple arteries including the middle meningeal artery (arrowhead)

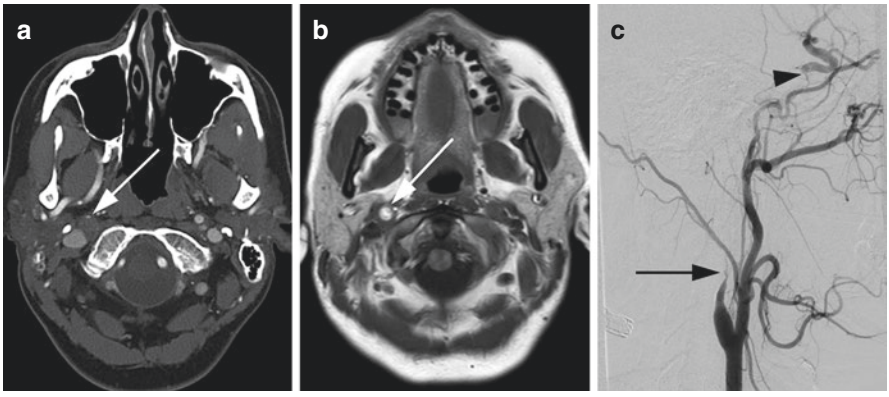

Fig. 2.9 External to internal carotid artery collateral flow. Patient with a right cervical ICA dissection. CTA showed a right ICA dissection with severe lumen narrowing (**a**, arrow). MRI showed a large T1-hyperintense intramural hematoma (**b**, arrow). DSA showed ICA dissection (arrow) along with ECA to intracranial ICA collateral flow (**c**, arrowhead)

access site for embolization of dural tumors (e.g. meningioma) or dAVF as seen in Fig. 2.8. The sphenopalatine branch in the pterygopalatine fossa supplies the deep face and nose, and provides embolization access to tumors in this region (e.g. juvenile angiofibroma) and for nosebleeds. There is also high potential for ECA-ICA collateral flow as shown in Fig. 2.9. Much like the STA, this vessel can be involved with deep face vasculitis (Fig. 2.10).

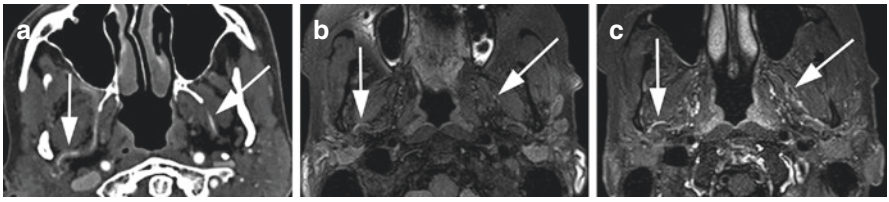

Fig. 2.10 Internal maxillary artery vasculitis. Patient presenting with facial pain and found to have eosinophilic vasculitis on biopsy. CTA showed bilateral internal maxillary artery lumen narrowing and wall thickening (**a**, arrows). MRI also showed wall thickening on T1 precontrast black blood images (**b**, arrows) and enhancement on postcontrast images (**c**, arrows)

Internal Carotid Artery (ICA)

The ICA is named for the more 'internal' path it takes throughout the neck. The first segment of the ICA is the cervical segment and this extends from the bifurcation to the skull base. Within this segment, the carotid bulb is an anatomic dilation measuring approximately 2 cm in length along the outer wall of the proximal ICA. The carotid bulb is particularly predisposed to atherosclerosis as discussed previously. Distal to the bifurcation, the ICA has been studied extensively with classification systems based on anatomy and clinical relevance.

ICA Anatomy

The ICA is divided up into multiple segments with some variation based on classification system. Fischer first devised the ICA segment classification in 1938, but named the segments C1-C5 from superior to inferior to identify skull base lesions based on mass effect on angiography (prior to cross sectional imaging). In 1996, the most widely used 'Modified Fischer Classification' system was devised by Bouthillier with 7 segments (C1-C7) from inferior to superior. This is the primary system used by neurointerventionalists today (Fig. 2.11).

Modified Fischer classification system The following is a description of the modified Fischer classification system used at many institutions. Imaging examples follow each segment description.

Cervical Segment (C1)

The first segment, or 'cervical' segment, extends from the carotid bifurcation to the carotid canal at the skull base. This segment has a rich supply of vasa vasorum centered at the carotid bifurcation and bulb. The cervical ICA is especially prone to

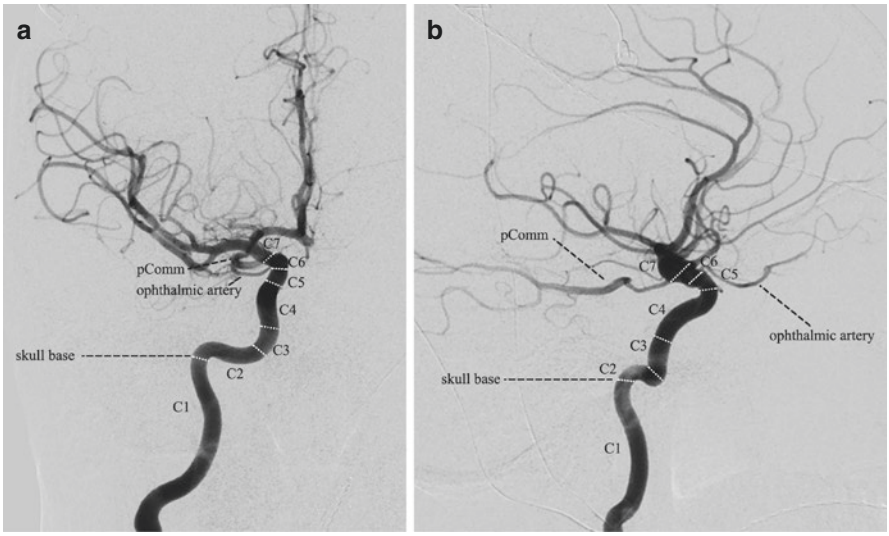

Fig. 2.11 Modified Fischer classification system. The Modified Fischer classification system is shown on frontal (**a**) and lateral (**b**) DSA projections with following segments: C1 – cervical, C2 – petrous, C3 – lacerum, C4 – cavernous, C5 – clinoid, C6 – ophthalmic, C7 – communicating. The skull base, ophthalmic artery and posterior communicating (pComm) arteries are labeled for reference

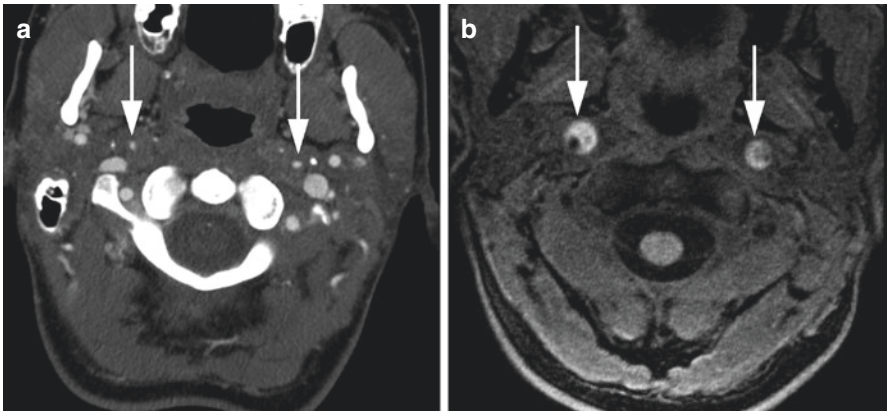

Fig. 2.12 Cervical internal carotid artery dissection. Patient with bilateral cervical ICA dissections. CTA (**a**) showed bilateral severe cervical ICA lumen narrowing (arrows). MRI T1-weighted images (**b**) demonstrated large bilateral T1-hyperintense intramural hematomas (arrows)

dissections, which can occur through direct intimal tear or ruptured vasa vasorum resulting in intramural hematoma. The cervical ICA is also prone to pathology from fibromuscular dysplasia, a form of collagen vascular disease. An example of bilateral cervical ICA dissections is shown in Fig. 2.12.

Petrous Segment (C2)

Once the vessel enters the skull base, it becomes the relatively long 'petrous' segment throughout the carotid canal in the petrous temporal bone. Atherosclerotic plaque, aneurysms, and dissections can occur along the petrous segment. Injury and dissection can occur from high velocity trauma from motor vehicle crashes and resultant skull base fractures. An example of a petrous ICA aneurysm in Fig. 2.13 and petrous ICA dissection in Fig. 2.14.

Lacerum Segment (C3)

After the petrous segment, the ICA extends up to the foramen lacerum where it becomes a short 'lacerum' segment. The petrolingual ligament surrounds a portion of the dorsolateral walls of the lacerum ICA segment, just under the anteroinferior portion of the anteromedial wall of the trigeminal cave [22]. While the lacerum segment is relatively short, the proximity to the foramen lacerum makes this segment especially prone to perivascular spread of disease from head and neck cancer or deep face infection, as shown in Fig. 2.15.

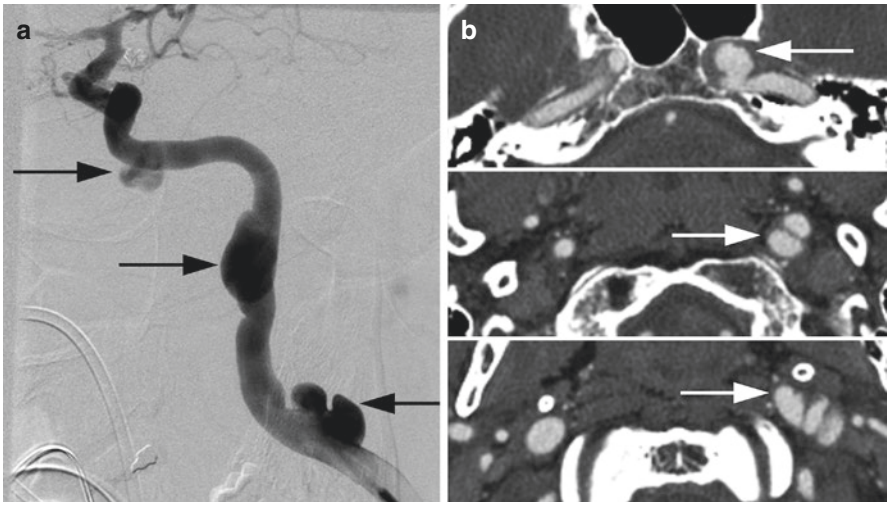

Fig. 2.13 Petrous internal carotid artery pseudoaneurysm. Patient with fibromuscular dysplasia and a petrous ICA pseudoaneurysm. DSA (**a**) and CTA (**b**) demonstrate multifocal cervical ICA lumen corrugation (lower arrow), cervical ICA pseudoaneurysm (middle arrow), and petrous ICA pseudoaneurysm (lower arrow)

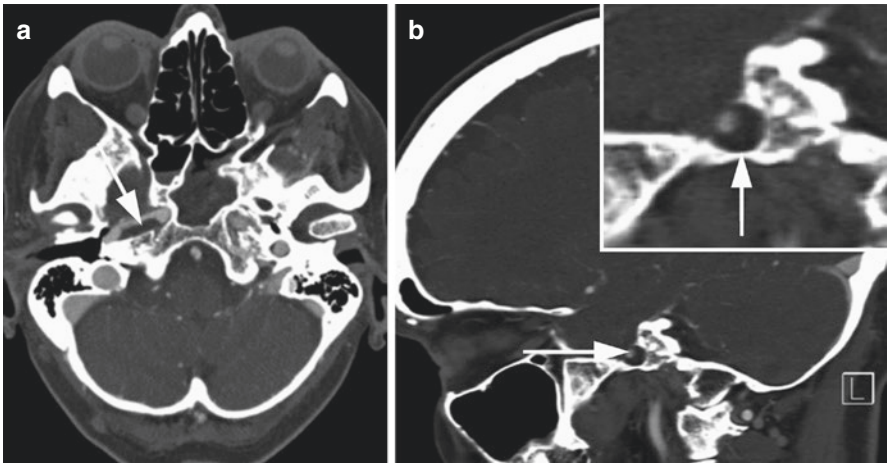

Fig. 2.14 Petrous internal carotid artery dissection. Patient presenting with right hemispheric stroke and right petrous ICA dissection. Axial (**a**) and sagittal (**b**, inset) CTA showed 50% lumen narrowing and intramural hematoma (arrows) indicating dissection of the right petrous ICA

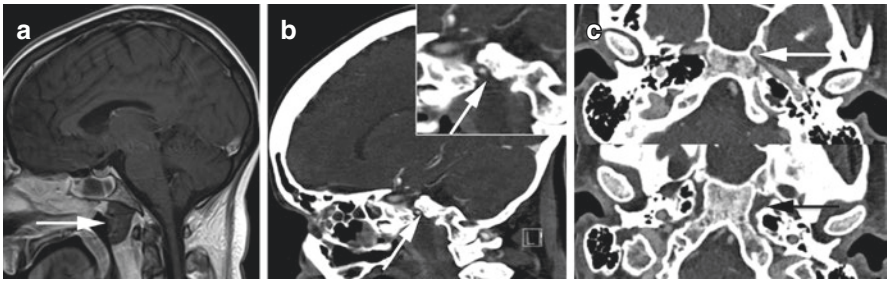

Fig. 2.15 Lacerum internal carotid artery perivascular spread of infection. Patient with intracranial spread of nasopharyngeal mucor infection. Sagittal T1 postcontrast MRI (**a**) shows marked nasopharyngeal mucosal thickening with central nonenhancing tissue extending to the clivus, compatible with vasoinvasive fungal disease (arrow). Sagittal (**b**, inset) CTA shows perivascular spread of infection through the foramen lacerum with narrowing of the ICA lumen (arrow). Axial CTA (**c**) also shows asymmetric narrowing of the ICA (C top, white arrow) and extension through the foramen lacerum (C bottom, black arrow)

Cavernous Segment (C4)

The ICA then passes under the petrolingual ligament, enters the cavernous sinus, and becomes a relatively long 'cavernous' segment from the posterior genu through the anterior genu. The cavernous segment has two important branches, the meningohypophyseal trunk (MHT) and inferolateral trunk (ILT), both of which serve as important access and potential treatment points for dAVF or meningiomas.

One of the most common findings in the cavernous ICA is calcification often identified by CT. Although there is some debate on the causes of these calcifications, significant correlations exist with diabetes, hypercholesterolemia, and hypertension and they are commonly seen alongside microangiopathic disease [23]. Cavernous ICA calcifications are also associated with atherosclerotic risk factors including age, sex, vascular risk factors, serum C-reactive protein, estimated glomerular filtration rate and homocysteine [24]. Still, the cavernous ICA can develop calcification even at teenagers and pathology specimens from children as young as 9 years old show this may relate to internal elastic lamina calcification in young otherwise healthy people [25]. This argues that at least some of the carotid siphon calcification is not related to atherosclerotic change. Furthermore, there are mixed results on the thromboembolic potential of cavernous ICA calcifications, with some studies finding that high-grade calcifications are associated with acute large and small vessel infarcts [26] and other studies showing no correlation between cavernous ICA calcifications and acute infarction [27] or white matter hyperintensities [28]. This segment is also associated with injuries related to high velocity or penetrating trauma, including dissection and AVF, due to its unique anatomy surrounded by cavernous venous sinusoids. An example of a direct CC fistula is shown in Fig. 2.16.

Lastly, the cavernous ICA accounts for 2–9% of intracranial aneurysms with a relatively small risk of subarachnoid hemorrhage (0.2–0.4% per year) given the

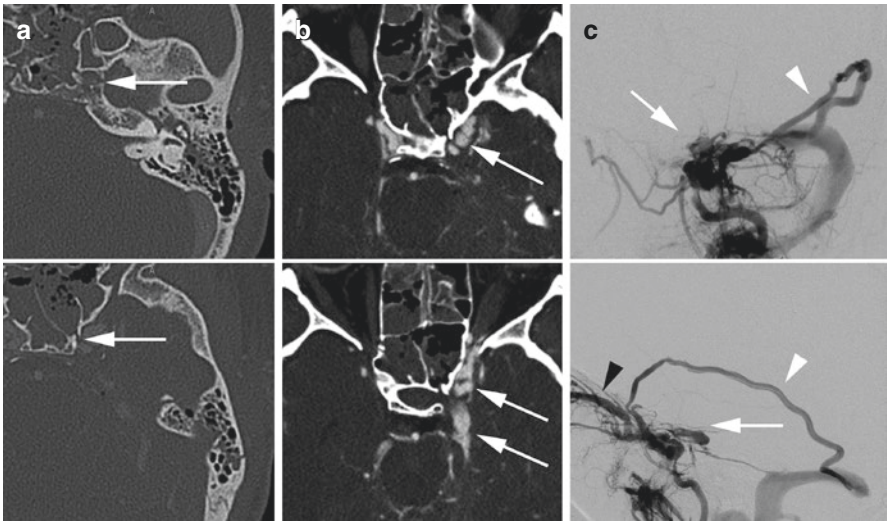

Fig. 2.16 Direct cavernous carotid fistula. Patient following a motor vehicle crash with skull base fractures and left cavernous carotid fistula. CT bone algorithm (**a**, top and bottom) demonstrates extensive skull base fractures through the sphenoid sinus and carotid canal (arrows). CTA (**b**, top and bottom) showed asymmetrically enlarged and irregular left cavernous sinus with arterial phase enhancement (arrows). DSA (**c**, top = frontal projection and bottom = lateral projection) confirmed a posttraumatic direct cavernous carotid fistula (arrow) with cervical ICA injection. Immediate venous contrast enhancement was present in the vein of Labbe (white arrowhead) extending into the sigmoid sinus as well as the superior ophthalmic vein (black arrowhead)

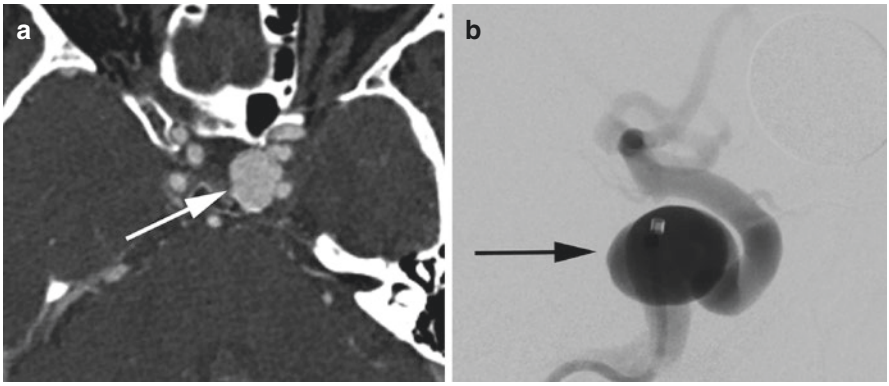

Fig. 2.17 Cavernous internal carotid artery aneurysm. Patient with a large cavernous ICA aneurysm. CTA (**a**) and DSA (**b**) show the large saccular aneurysm involving the cavernous ICA segment (arrows)

location in the cavernous sinus. Still, novel treatments have evolved to cover giant aneurysms in this location which can erode into adjacent structures and cause symptoms from mass effect [29]. An example of a cavernous ICA aneurysm is shown in Fig. 2.17. Further, perivascular spread of sinus disease can occur in this segment, with an example of perivascular spread of sphenoid sinus infection along the cavernous ICA is shown in Fig. 2.18.

Clinoid Segment (C5)

After the anterior genu of the cavernous segment, the ICA passes through the proximal dural ring and becomes a relatively short segment at the level of the clinoid process, the 'clinoid' segment. At this point, the ICA travels through the distal dural ring and becomes subarachnoid. This segment is relatively short, but also an important site of pathology including atherosclerosis, vessel injury and aneurysm, with an example in Fig. 2.19. Special consideration must be given to the 'carotid cave', a subsegment occurring along the medial aspect of the ICA between the clinoid and ophthalmic segments, where a redundant portion of the distal dural ring can project inferiorly into the cavernous sinus. Aneurysms here are *intradural*, but can appear extradural on angiographic imaging Fig. 2.20.

Ophthalmic Segment (C6)

The ophthalmic artery origin occurs just after the distal dural ring, and at this point becomes the 'ophthalmic' segment up to the origin of the posterior communicating artery. This is the site for ophthalmic aneurysms, which occur at the junction of the

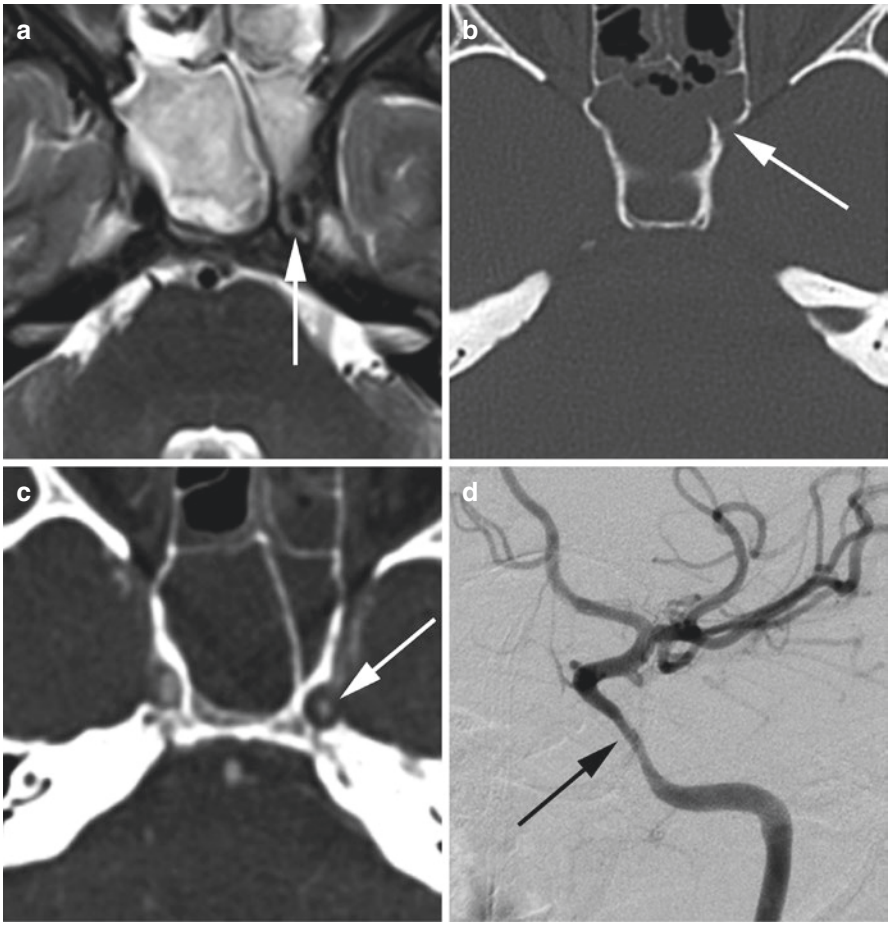

Fig. 2.18 Cavernous internal carotid artery perivascular spread of infection. Patient presenting with headache was evaluated initially with a noncontrast MRI. MRI T2-weighted images (**a**) showed completely opacified sphenoid sinuses and adjacent narrowing of the left cavernous ICA flow void (arrow). CT bone algorithm (**b**) showed dehiscence along the left sphenoid sinus (arrow) with adjacent narrowing of the left cavernous ICA on CTA (**c**, arrow). DSA (**d**) confirmed fusiform narrowing of the left cavernous ICA (arrow). Further testing revealed fusibacterium necrophorum infection of the sphenoid sinuses

ophthalmic artery origin and adjacent ICA (Fig. 2.21). This segment can also be injured along the dorsal ICA, forming the important do-not-miss 'blister' aneurysm or pseudoaneurysm associated with rapid growth rate and high morbidity and mortality (Fig. 2.22).

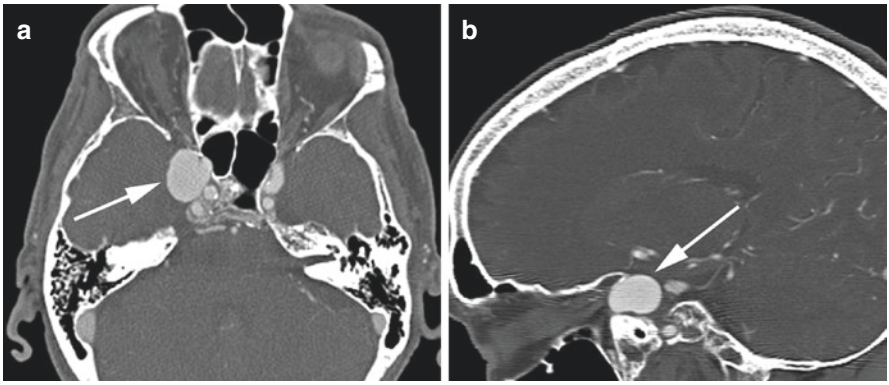

Fig. 2.19 Clinoid internal carotid artery aneurysm. Patient with a clinoid segment ICA aneurysm. Axial (**a**) and sagittal (**b**) CTA demonstrates a large aneurysm involving the clinoid ICA segment (arrows)

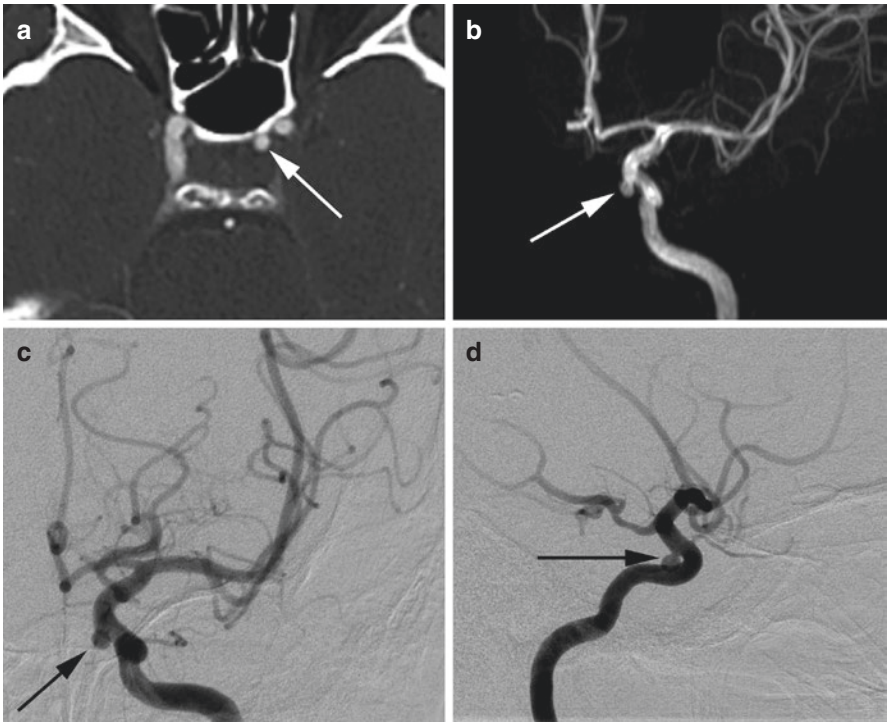

Fig. 2.20 Carotid cave aneurysm. Patient with a left carotid cave aneurysm. CTA (**a**), time-of-flight MRA 3D reformat (**b**), DSA frontal (**c**) and lateral projections (**d**) show a small ICA aneurysm involving the carotid cave (arrow). A carotid cave aneurysm is intradural, but may appear extradural due to inferomedial projection into the cavernous sinus

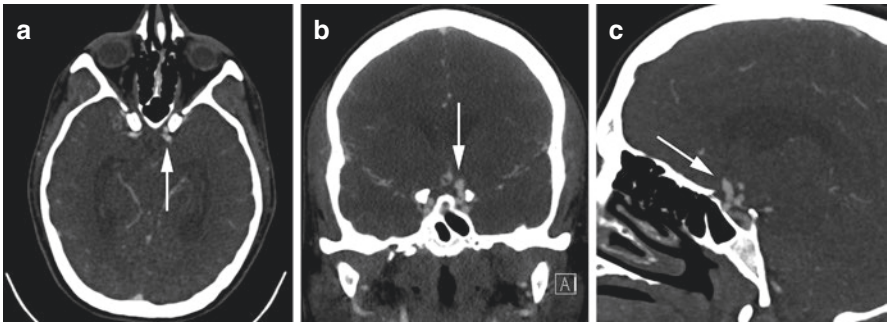

Fig. 2.21 Ophthalmic segment aneurysm. Patient with a left ophthalmic segment aneurysm. Axial (**a**), coronal (**b**) and sagittal (**c**) CTA showing a superiorly projecting left ICA ophthalmic segment aneurysm (arrow)

Communicating Segment (C7)

The terminal ICA segment extends from the posterior communicating artery origin to the ICA terminus and is known as the 'communicating' segment. This segment includes the anterior choroidal artery, which supplies the posterior limb of the internal capsule [30, 31]. Anterior choroidal aneurysms (Fig. 2.23), posterior communicating artery aneurysms (Fig. 2.24) and fusiform aneurysms such as can be seen with HIV vasculopathy (Fig. 2.25) can occur in this segment. At the ICA terminus the vessel divides into the MCA M1 and ACA A1 segments, and from these originate deep brain perforators including both the medial and lateral lenticulostriates supplying the caudate and putamen.

ICA Anatomic Variants

Persistent Carotid-Basilar Anastomoses

There are 4 potential variant anastomoses between the ICA and vertebral artery not including the posterior communicating artery. The most common of these is the persistent trigeminal artery with a lateral or medial course (**Saltzman type I or II**) that occurs in 0.1–0.2% of the population [32]. The second most common is the persistent hypoglossal artery (0.03–0.09%), which arises from the ICA at C1-C2 and passes through the hypoglossal canal to join the basilar artery. The proatlantal intersegmental artery is the third most common variant and arises from the cervical ICA at C2-C3 and joins with a vertebral artery or more rarely ECA to vertebral artery at the craniocervical junction. The fourth variant, the persistent otic artery is extremely rare and connects the petrous ICA to basilar artery through the internal auditory canal.

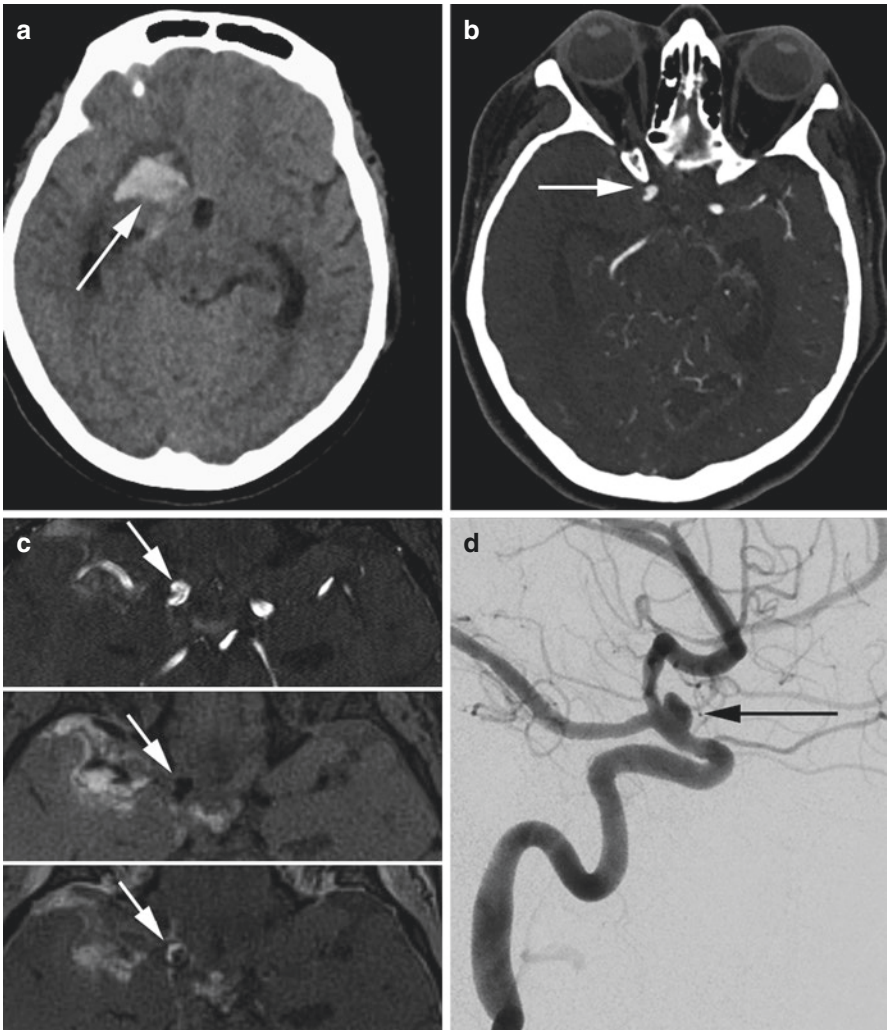

Fig. 2.22 Dorsal variant internal carotid artery pseudoaneurysm. Patient with intraparenchymal and subarachnoid hemorrhage on initial CT scan (**a**). Axial CTA (**b**) shows a right ICA ophthalmic segment blister aneurysm (arrow). Vessel wall imaging was performed with the aneurysm (arrow) on time-of-flight (**c**, top), flow suppressed T1 precontrast (**c**, middle), and with vessel wall enhancement flow suppressed T1 postcontrast (**c**, bottom). DSA (**d**) confirms a dorsal variant ICA pseudoaneurysm (arrow)

Often one clue to the existence of a carotid-basilar anastomosis is a small vertebrobasilar system that abruptly changes to normal caliber, with the anastomosis found on close inspection. One must also search for other variants, since aneurysms are reported in up to 15% of cases as are other anomalies including fenestrations, absent vessels or dAVF. These anomalies are most often asymptomatic and treatment is not required unless there is an associated aneurysm or fistula.

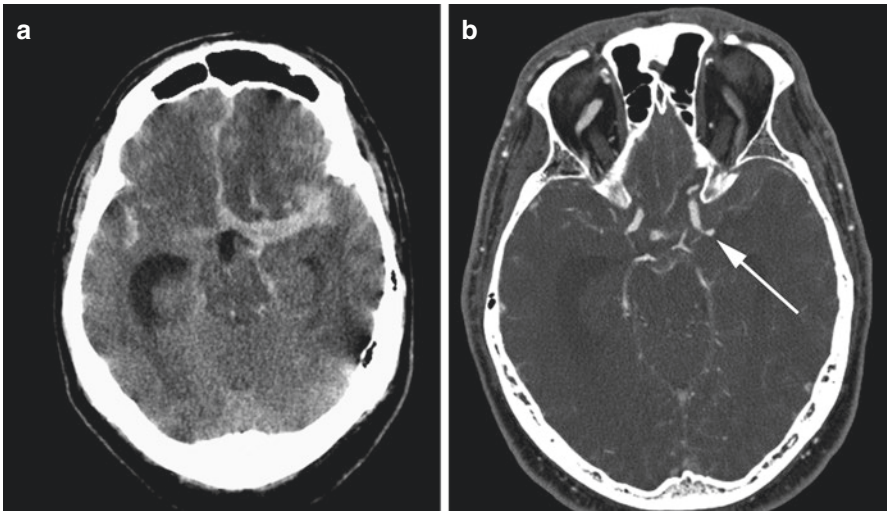

Fig. 2.23 Anterior choroidal aneurysm. Patient presenting with acute subarachnoid hemorrhage asymmetric to the left on noncontrast CT (**a**). CTA (**b**) showed a recently ruptured anterior choroidal artery aneurysm (arrow)

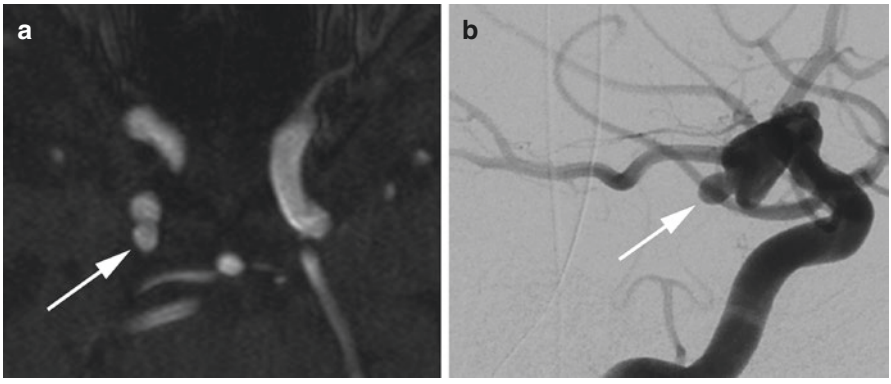

Fig. 2.24 Posterior communicating artery aneurysm. Patient with a right-sided posterior communicating artery aneurysm. Time-of-flight MRA (**a**) and DSA (**b**) demonstrate a wide-necked, irregular 7 × 8 mm posterior communicating artery aneurysm with an associated daughter sac (arrow)

Aberrant ICA

This congenital variant results from failed formation of the extracranial ICA and is actually formed by a collateral pathway from the ascending pharyngeal artery to the inferior tympanic artery then the caroticotympanic artery, finally connecting with the posterolateral petrous ICA. On axial CTA, the aberrant ICA crosses the middle ear from posterior to anterior, with an associated enlarged tympanic canaliculus located anteromedial to the stylomastoid foramen/mastoid segment of the facial

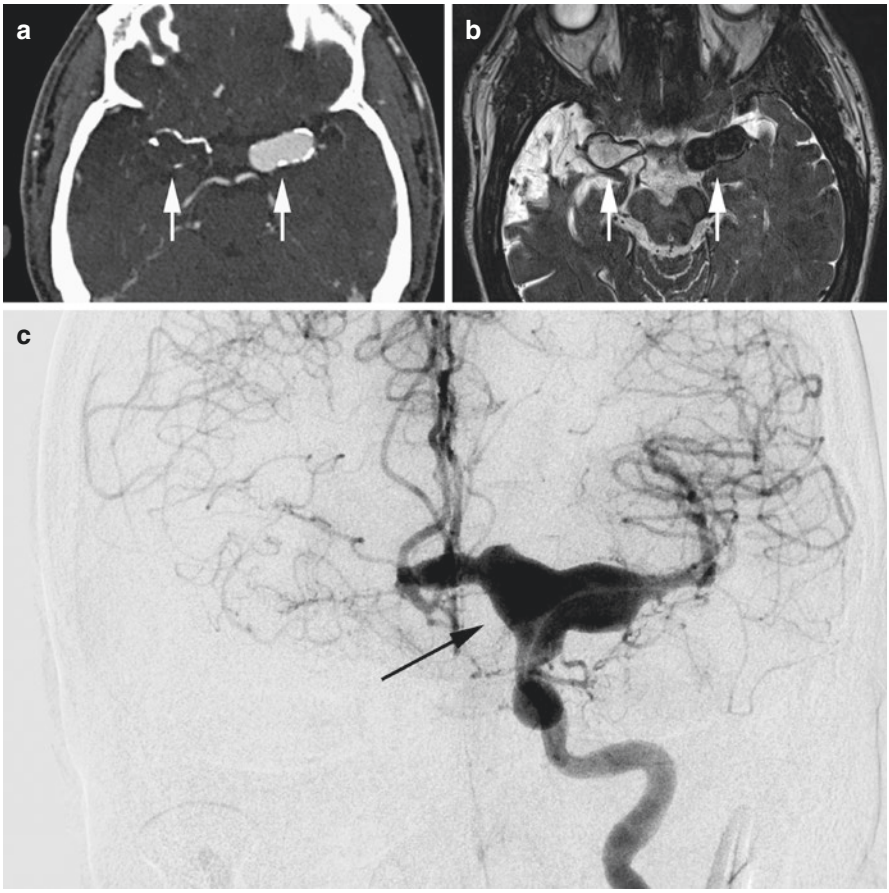

Fig. 2.25 Carotid terminus vasculopathy related to HIV. Patient with longstanding HIV. CTA (**a**) and T2-weighted MRI (**b**) demonstrate fusiform aneurysms involving the bilateral carotid termini (arrows) with occlusion on the right. DSA with left ICA injection (**c**) shows fusiform dilation of the carotid terminus, A1 ACA and M1 MCA segments (arrow)

nerve. 30% have an associated persistent stapedial artery with an absent foramen spinosum and an enlarged anterior tympanic segment of the facial nerve on CT. While often asymptomatic and incidentally found on CTA or otoscopy, these can be associated with pulsatile tinnitus and conductive hearing loss.

Lateral ICA

In this rare variant along the temporal bone, the ICA enters the anterior middle ear cavity more lateral than normal as can be seen in Fig. 2.26. By definition, if the petrous ICA is lateral to the mid cochlea on axial images, the ICA is lateralized.

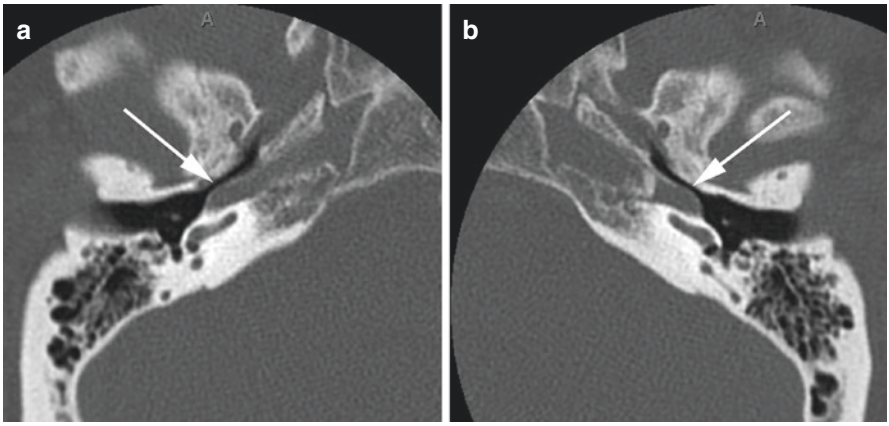

Fig. 2.26 Lateralized internal carotid artery. Patient with asymptomatic bilateral lateralized ICA's. Noncontrast CT of the temporal bones right (**a**) and left (**b**) ICA's coursing along the cochlear promontories (arrows), but without a persistent stapedial artery or enlarged tympanic canaliculus

Often the lateral ICA osseous covering is dehiscent and this can mimic aberrant ICA on MIP images. With a lateral ICA, there is no association with a persistent stapedial artery and the inferior tympanic canaliculus is not enlarged. These are often asymptomatic incidental findings on CTA or otoscopic exam, though some patients can present with pulsatile tinnitus.

Summary

In conclusion, the carotid artery is an important conduit for blood supply to the brain, face and neck. Carotid artery anatomy forms the basis of plaque formation and affects downstream stroke risk. An intricate knowledge is essential for appropriate surgical and endovascular treatment planning.

References

1. Nguyen RP, Shah LM, Quigley EP, Harnsberger HR, Wiggins RH. Carotid body detection on ct angiography. AJNR Am J Neuroradiol. 2011;32:1096–9.
2. Rupprecht S, Finn S, Ehrhardt J, Hoyer D, Mayer T, Zanow J, et al. Autonomic outcome is better after endarterectomy than after stenting in patients with asymptomatic carotid stenosis. J Vasc Surg. 2016;64:975–84.
3. Schrag B, Vaucher P, Bollmann MD, Mangin P. Death caused by cardioinhibitory reflex cardiac arrest–a systematic review of cases. Forensic Sci Int. 2011;207:77–83.
4. Bo WJ, McKinney WM, Bowden RL. The origin and distribution of vasa vasorum at the bifurcation of the common carotid artery with atherosclerosis. Stroke. 1989;20:1484–7.

5. Boyle EC, Sedding DG, Haverich A. Targeting vasa vasorum dysfunction to prevent atherosclerosis. Vasc Pharmacol. 2017;96–98:5–10.
6. Harrison DG, Widder J, Grumbach I, Chen W, Weber M, Searles C. Endothelial mechanotransduction, nitric oxide and vascular inflammation. J Intern Med. 2006;259:351–63.
7. Moore JE Jr, Xu C, Glagov S, Zarins CK, Ku DN. Fluid wall shear stress measurements in a model of the human abdominal aorta: oscillatory behavior and relationship to atherosclerosis. Atherosclerosis. 1994;110:225–40.
8. Moyna NM, Thompson PD. The effect of physical activity on endothelial function in man. Acta Physiol Scand. 2004;180:113–23.
9. Traub O, Berk BC. Laminar shear stress: mechanisms by which endothelial cells transduce an atheroprotective force. Arterioscler Thromb Vasc Biol. 1998;18:677–85.
10. Smart EJ, Ying YS, Conrad PA, Anderson RG. Caveolin moves from caveolae to the golgi apparatus in response to cholesterol oxidation. J Cell Biol. 1994;127:1185–97.
11. Koller A, Huang A. Shear stress-induced dilation is attenuated in skeletal muscle arterioles of hypertensive rats. Hypertension. 1995;25:758–63.
12. Ku DN, Giddens DP, Zarins CK, Glagov S. Pulsatile flow and atherosclerosis in the human carotid bifurcation. Positive correlation between plaque location and low oscillating shear stress. Arteriosclerosis. 1985;5:293–302.
13. Asakura T, Karino T. Flow patterns and spatial distribution of atherosclerotic lesions in human coronary arteries. Circ Res. 1990;66:1045–66.
14. De Keulenaer GW, Chappell DC, Ishizaka N, Nerem RM, Alexander RW, Griendling KK. Oscillatory and steady laminar shear stress differentially affect human endothelial redox state: role of a superoxide-producing nadh oxidase. Circ Res. 1998;82:1094–101.
15. McNally JS, Davis ME, Giddens DP, Saha A, Hwang J, Dikalov S, et al. Role of xanthine oxidoreductase and nad(p)h oxidase in endothelial superoxide production in response to oscillatory shear stress. Am J Physiol Heart Circ Physiol. 2003;285:H2290–7.
16. Hwang J, Saha A, Boo YC, Sorescu GP, McNally JS, Holland SM, et al. Oscillatory shear stress stimulates endothelial production of o2- from p47phox-dependent nad(p)h oxidases, leading to monocyte adhesion. J Biol Chem. 2003;278:47291–8.
17. Cai H, McNally JS, Weber M, Harrison DG. Oscillatory shear stress upregulation of endothelial nitric oxide synthase requires intracellular hydrogen peroxide and camkii. J Mol Cell Cardiol. 2004;37:121–5.
18. Hanneman K, Newman B, Chan F. Congenital variants and anomalies of the aortic arch. Radiographics. 2017;37:32–51.
19. Krejza J, Arkuszewski M, Kasner SE, Weigele J, Ustymowicz A, Hurst RW, et al. Carotid artery diameter in men and women and the relation to body and neck size. Stroke. 2006;37:1103–5.
20. Geibprasert S, Pongpech S, Armstrong D, Krings T. Dangerous extracranial-intracranial anastomoses and supply to the cranial nerves: vessels the neurointerventionalist needs to know. AJNR Am J Neuroradiol. 2009;30:1459–68.
21. James RF, Kramer DR, Page PS, Gaughen JR Jr, Martin LB, Mack WJ. Strategic and technical considerations for the endovascular embolization of intracranial meningiomas. Neurosurg Clin N Am. 2016;27:155–66.
22. Liu XD, Xu QW, Che XM, Mao RL. Anatomy of the petrosphenoidal and petrolingual ligaments at the petrous apex. Clin Anat. 2009;22:302–6.
23. Ptak T, Hunter GH, Avakian R, Novelline RA. Clinical significance of cavernous carotid calcifications encountered on head computed tomography scans performed on patients seen in the emergency department. J Comput Assist Tomogr. 2003;27:505–9.
24. Kim JM, Park KY, Shin DW, Park MS, Kwon OS. Relation of serum homocysteine levels to cerebral artery calcification and atherosclerosis. Atherosclerosis. 2016;254:200–4.
25. Bergevin MA, Daugherty CC, Bove KE, McAdams AJ. The internal carotid artery siphon in children and adolescents. Hum Pathol. 1991;22:603–6.

26. Erbay S, Han R, Baccei S, Krakov W, Zou KH, Bhadelia R, et al. Intracranial carotid artery calcification on head ct and its association with ischemic changes on brain mri in patients presenting with stroke-like symptoms: retrospective analysis. Neuroradiology. 2007;49:27–33.
27. Babiarz LS, Yousem DM, Bilker W, Wasserman BA. Middle cerebral artery infarction: relationship of cavernous carotid artery calcification. AJNR Am J Neuroradiol. 2005;26:1505–11.
28. Babiarz LS, Yousem DM, Wasserman BA, Wu C, Bilker W, Beauchamp NJ Jr. Cavernous carotid artery calcification and white matter ischemia. AJNR Am J Neuroradiol. 2003;24:872–7.
29. Ambekar S, Madhugiri V, Sharma M, Cuellar H, Nanda A. Evolution of management strategies for cavernous carotid aneurysms: a review. World Neurosurg. 2014;82:1077–85.
30. Alqahtani SA, Luby M, Nadareishvili Z, Benson RT, Hsia AW, Leigh R, et al. Perfusion deficits and association with clinical outcome in patients with anterior choroidal artery stroke. J Stroke Cerebrovasc Dis. 2017;26:1755–9.
31. Nadaf S, Chakor RT, Kothari KV, Patel BA. Anterior choroidal artery infarction. BMJ Case Rep. 2018;2018:bcr-2017.
32. Alcala-Cerra G, Tubbs RS, Nino-Hernandez LM. Anatomical features and clinical relevance of a persistent trigeminal artery. Surg Neurol Int. 2012;3:111.